PCCP

ROYAL SOCIETY OF CHEMISTRY

PAPER

View Article Online
View Journal | View Issue

Cite this: *Phys. Chem. Chem. Phys.*, 2025, **27**, 18760

# The role of oxygen in the synthesis of the $Mo_2CT_x$ MXene from the $Mo_2Ga_2C$ MAX phase

José D. Gouveia *[a] and José R. B. Gomes *[b]

MAX phases are layered materials that have been known for over 60 years and MXenes are their metaphorical children, a family of two-dimensional (2D) materials that appeared in 2011. MXenes are often synthesised by etching out the layers of the A element of their parent MAX phases. The remaining 2D MXene layers are very reactive and spontaneously become covered by a layer called the surface termination. The $Mo_2C$ MXene was first synthesised in 2015, by using hydrofluoric acid to remove the Ga layers from the $Mo_2Ga_2C$ MAX phase, and its surface termination was determined to be mostly composed by O groups. While the layers of Mo and C in $Mo_2Ga_2C$ are arranged in a face-centred cubic manner, those of $Mo_2C$ prefer a hexagonal close-packed stacking. This implies that, at some point during the etching process, a phase transition should occur because of the replacement of Ga by O. Herein, we employ density–functional theory calculations to analyse the thermodynamics of this process by assessing the stability of the two stacking phases of the $Mo_2Ga_2C$ MAX phase, as the Ga atoms are gradually replaced by O ones. Among other results, we identify the preferred locations of O and F atoms in the $Mo_2Ga_2C$ lattice, propose a possible explanation for the greater presence of O atoms over F ones on the surface of as-synthesised $Mo_2C$ MXenes, evaluate the interaction between O atoms in $Mo_2Ga_2C$ crystals, estimate the energy of Ga–Ga bonds, and lastly, show that the relative stability of the two stacking phases of $Mo_2Ga_2C$ is reversed when approximately half of the Ga content is replaced by O.

Received 17th June 2025,
Accepted 11th August 2025

DOI: 10.1039/d5cp02315g

rsc.li/pccp

## Introduction

MAX phases and MXenes are two families of layered materials that are inexorably connected. The stoichiometry of the former (three-dimensional solids) can traditionally be written as $M_{n+1}AX_n$ ($n$ = 1 to 4), where M is an early transition metal, A is an element usually from groups 13 or 14 of the Periodic Table of the Elements, and X is carbon and/or nitrogen.[1] Structurally, $n$ + 1 layers of the M element, intercalated by $n$ layers of the X element in a face-centred cubic (FCC) arrangement (distorted $XM_6$ octahedra), are separated by single flat layers of the A element. MXenes are the two-dimensional (2D) derivatives of MAX phases, obtained by etching out the A layers of their parent structures, and retaining only the $M_{n+1}X_n$ scaffold.[2,3] The outermost layers of these 2D materials comprise M atoms and are very reactive, so that the stoichiometry of as-synthesised MXenes is in fact $M_{n+1}X_nT_x$, where T is the surface termination, whose composition (most commonly –O, –F and –OH groups) depends on the synthesis conditions. The first MXene, $Ti_3C_2$, was synthesised from the $Ti_3AlC_2$ MAX phase, from which the Al atoms were removed in the form of aluminium fluoride ($AlF_3$).[2]

While MAX phases have been known for over 60 years[4] and more than 300 different ones have been produced,[1] accounting for multiple $n$ and M, A and X element combinations, MXenes are a relatively new family, with only a few tens of members realized, although hundreds have been predicted to be stable.[3] MXenes display high electrical conductivity, mechanical robustness, and tuneability inherited from MAX phases. Being 2D, MXenes find application in sensing,[5–8] catalysis,[9–12] hydrogen storage,[13–15] electronics and photonics,[16] among others.[17–19]

Since MXenes are mostly obtained from MAX phases, the interest in synthesizing new MXenes has in turn motivated the synthesis of novel MAX phases, as may have happened in the search for the $Mo_2C$ MXene. The $Mo_2GaC$ MAX phase was first reported in 1967,[20] but the removal of the Ga layers from it to form the $Mo_2C$ MXene has proven very challenging thus far. However, in 2015, four years after the introduction of MXenes, a new layered material, with stoichiometry $Mo_2Ga_2C$, was discovered.[21] This was assumed to be the first of a new family, but some authors simply call it a double A-layer MAX phase. Since then, at least 10 different double A-layer MAX phases,

---

[a] *CICECO-Aveiro Institute of Materials, Department of Physics, University of Aveiro, Campus Universitário de Santiago, 3810-193 Aveiro, Portugal. E-mail: gouveia@ua.pt*
[b] *CICECO-Aveiro Institute of Materials, Department of Chemistry, University of Aveiro, Campus Universitário de Santiago, 3810-193 Aveiro, Portugal. E-mail: jrgomes@ua.pt*

with stoichiometries $M_2A_2X$ and $M_3A_2X_2$, have been reported, but $Mo_2Ga_2C$ is the only one that was realized by direct synthesis, rather than by modifying existing MAX phases.[1] The $Mo_2Ga_2C$ MAX phase is an unusual one, not only for having two layers of the A element per formula unit, but also for the fact that these two layers sit exactly on top of each other, instead of a close-packed fashion.[21] In the same year that $Mo_2Ga_2C$ was discovered, the same group was finally able to synthesize the $Mo_2C$ MXene,[22] representing both the first Mo-based MXene to be made and the first MXene to be derived from a non-Al MAX phase. The $Mo_2C$ MXene was attained in the most usual way, *i.e.*, by immersing the parent $Mo_2Ga_2C$ MAX phase in 50% concentrated hydrofluoric acid for a few hours at 50 °C, resulting in the effective removal of almost all the Ga content. In the same work, this procedure was also attempted on $Mo_2GaC$ MAX phase samples, but unsuccessfully. For this reason, since then, all subsequent syntheses of the $Mo_2C$ MXene are performed from the double A-layer MAX phase, $Mo_2Ga_2C$, even when employing hydrothermal routes involving 24-hour etching with LiF + HCl, NaF/KF + HCl, or $NH_4F$ + HCl solutions at temperatures ranging from 140 to 180 °C.[23] The as-synthesised $Mo_2CT_x$ MXene had an approximate Mo : Ga : O : F content of 50 : 5 : 40 : 5.[22] In other words, it contained little Ga, as intended, and exhibited a surface termination dominated by oxygen atoms.

The transition from the $Mo_2Ga_2C$ MAX phase to the $Mo_2CT_x$ MXene is a curious one, since the $Mo_2C$ atomic layers in the MAX phase are known to be arranged in an FCC manner (also known as ABC stacking),[24,25] whereas the $Mo_2CT_x$ MXenes have their atomic layers arranged in a hexagonal close-packed structure (also known as ABA stacking), regardless of the composition of the surface termination.[12,26,27] This raises several questions. For example, is the $Mo_2Ga_2C$ MAX phase (*meta*)stable in an ABA stacking phase? Can the replacement of Ga atoms by O ones drive the transition from the ABC to the ABA atomic layer stacking? In this work, we answer these questions by performing density-functional theory (DFT) calculations to study the interaction of the $Mo_2Ga_2C$ MAX phase with oxygen and fluorine atoms, and by comparing the relative stability of the ABC and ABA stacking sequences in $Mo_2Ga_2C$ MAX phase models with varying degrees of Ga-to-O substitution.

## Computational method

We performed spin-polarized DFT calculations using the VASP code[28] and the PBE exchange–correlation functional, within the generalized gradient approximation.[29] The explicitly treated electrons were Mo: $4p^6$ $4d^5$ $5s^1$, Ga: $3d^{10}$ $4s^2$ $4p^1$, C: $2s^2$ $2p^2$, and O: $2s^2$ $2p^4$. The remaining core electrons were implicitly considered through the projector augmented-wave method.[30] Given that we are studying the transition from a three-dimensional MAX phase to two-dimensional MXene layers, it is expected that van der Waals interactions become relevant, at least between neighbouring MXene surfaces, so we investigated how some of our results change when D3 dispersion corrections[31] are included in the calculations. The PBE(-D3) approach is employed in this work to ensure consistency and enable direct comparison with values reported in the literature, as it is the most commonly used functional in computational studies of MXenes.[32] Given that both the $Mo_2Ga_2C$ MAX phase and the $Mo_2C$ MXene are known to exhibit metallic behavior, the use of higher-level functionals, such as hybrid approaches, would not alter their classification as metals, while other calculated properties would likely remain largely unchanged, though at significantly increased computational cost. Recent comparative studies of dispersion-corrected functionals, including PBE-TS, PBE-D2, PBE-D3, vdW-DF, vdW-DF2, optB88-vdW, and optB86b-vdW approaches, have identified PBE-D3 as the most accurate for computing out-of-plane lattice parameters,[33] and binding energies[34] in related transition-metal dichalcogenides. These findings further support the choice of computational methodology adopted in this work.

In our calculations, we used periodic models of different sizes (Fig. 1) and different simulation parameters for different purposes. We performed three types of calculations. In a first stage (1), we considered single unit cells of $Mo_2Ga_2C$ or $Mo_2CO_2$, with ABC or ABA atomic layer stacking, and calculated their lattice parameters, relative stability and electronic band diagrams. Then, in the second stage (2), we studied the interaction between $Mo_2Ga_2C$ and O or F atoms, as well as the interaction between substitutional O atoms in $Mo_2Ga_2C$. In the last stage (3), we investigated how the relative stability of ABC- and ABA-stacked $Mo_2Ga_2C$ changes with an increasing amount of substitutional O. The simulation parameters resulted from preliminary tests ensuring that relative energies are converged within less than 1 meV per atom and maximizing accuracy/efficiency trade-off, and are the following:

(1) Unit cell calculations were conducted to obtain lattice parameters and electronic band diagrams of pristine $Mo_2Ga_2C$ and $Mo_2CO_2$. Each model of a unit cell contains two formula units and D3 dispersion corrections were included in the $Mo_2CO_2$ MXene calculations. A large energy cutoff of 550 eV was employed, and tight atomic and electronic relaxation criteria were adopted as well, namely 5 meV $\text{Å}^{-1}$ and 1 μeV, respectively. The Brillouin zones were sampled using $\Gamma$-centred 15 × 15 × 3 grids of special $k$ points for the calculations of lattice parameters.[35] The energy band diagrams were calculated using an explicit list of $k$ points interpolated between high-symmetry points of the Brillouin zone of each material.

(2) The analysis of point defects in $Mo_2Ga_2C$ requires the use of larger models to partially screen unwanted interaction between periodic copies of each defect. Thus, we built supercells made of 4 × 4 × 1 unit cells of $Mo_2Ga_2C$, ensuring a separation of at least 12 Å between the periodic copies. Here, we used an energy cutoff of 415 eV, and atomic and electronic relaxation criteria of 0.01 eV $\text{Å}^{-1}$ and 0.01 meV, respectively. A $\Gamma$-centred grid with 3 × 3 × 3 special $k$ points was used to sample the Brillouin zones.[35]

(3) The assessment of how the relative stability of ABC- and ABA-stacked $Mo_2Ga_2C$ is modified as the concentration of substitutional O increases was done on models comprising

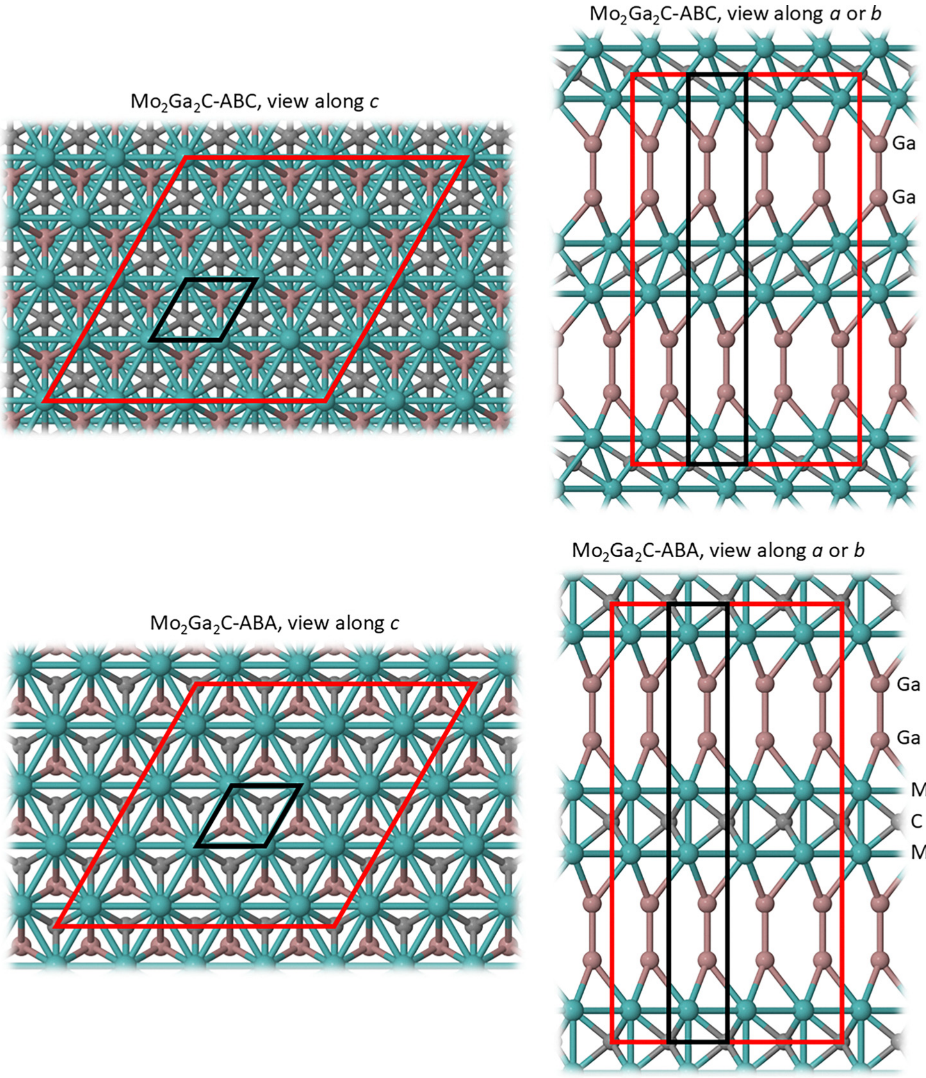

Fig. 1 Views of models of a unit cell (black lines) and a 4 × 4 supercell (red lines) of $Mo_2Ga_2C$ used in this work, with ABC (ABA) stacking shown in the top (bottom) panels. The models of the $Mo_2CO_2$ MXene with ABC and ABA atomic layer stacking are analogous to the ones of $Mo_2Ga_2C$ with the same stacking, with the Ga atoms replaced by O ones. The panels on the left show views along the *c* lattice vector, whereas the ones on the right show views along the *a* or *b* lattice vectors (the *a* and *b* directions are equivalent). Colour code for the spheres: Mo in cyan, Ga in pink, C in grey.

2 × 2 × 1 unit cells of $Mo_2Ga_2C$. Furthermore, the calculations were done separately in three ways to enable comparison of the results from each procedure: (i) with the PBE functional (without D3 corrections) and a fixed supercell size, (ii) with D3 corrections and fixed supercell size, and (iii) with D3 corrections and optimization of the supercell size for each O concentration. Here, we used the same energy cutoff and convergence criteria as in the study of point defects, and a $\Gamma$-centred grid with 7 × 7 × 3 special *k* points was used to sample the Brillouin zones.[35]

The formation energies, $E_{\text{form}}$, of defects involving a single O or F atoms in $Mo_2Ga_2C$ were calculated as

$$E_{\text{form}} = E_{\text{defect}} - E_{\text{pristine}} + E_{\text{removed}} - E_{\text{added}} \qquad (1)$$

Here, $E_{\text{defect}}$ and $E_{\text{pristine}}$ are the total energies of a supercell containing 4 × 4 × 1 unit cells of defective or pristine $Mo_2Ga_2C$, respectively. The quantities $E_{\text{removed}}$ and $E_{\text{added}}$ are the energies of the atoms that were removed or added to create the defect, respectively. In the case of interstitial defects, $E_{\text{removed}}$ is zero. The energies of a single Ga, C or O atom were calculated as the total energy per atom of a Ga bulk orthorhombic unit cell, a diamond unit cell, or an $O_2$ molecule. The energy of an F atom was calculated by subtracting half the energy of an $H_2$ molecule from that of an HF one, because the process of etching out the Ga layers from $Mo_2Ga_2C$ uses HF as a reagent. The energies of the isolated molecules were obtained by optimizing them in an asymmetric box with dimensions 10 × 11 × 12 Å, employing $\Gamma$-point sampling.

## Results and discussion

### Pristine $Mo_2Ga_2C$ MAX phase and $Mo_2CO_2$ MXene

The structure of $Mo_2Ga_2C$ (with the usual ABC stacking of its atomic layers) can be described as ABC-stacked $Mo_2C$ MXenes

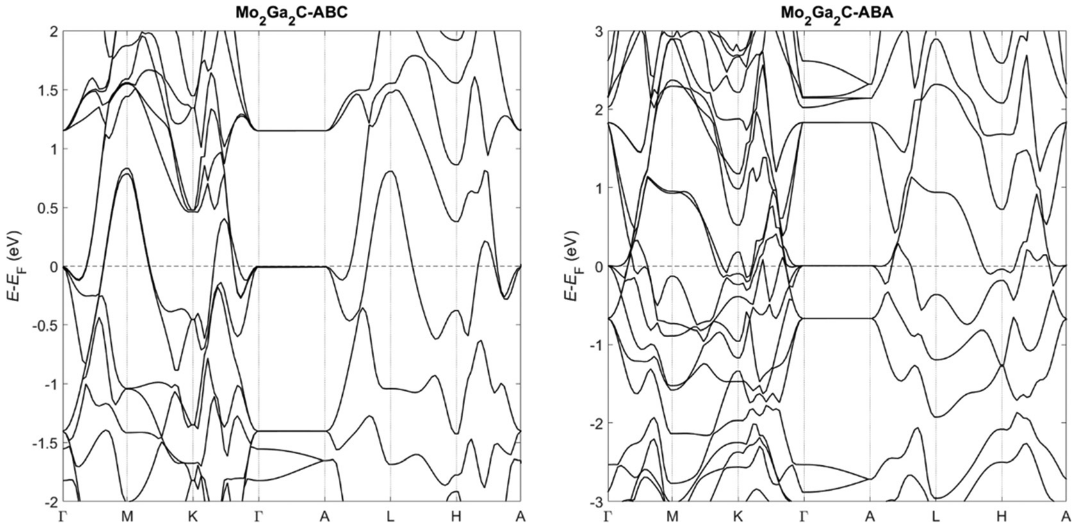

Fig. 2 Calculated band structure of $Mo_2Ga_2C$. The horizontal dashed line lies at the Fermi energy.

connected to each other by pairs of Ga atoms, in which the Ga–Ga bonds are perpendicular to the basal plane. The $Mo_2Ga_2C$-ABA can be described in an analogous way, but the $Mo_2C$ sections are aligned in an ABA fashion instead. Several relative alignments of the $Mo_2C$ layers and of the Ga layers along the direction of the $c$ lattice vector are possible, and the thermodynamic stability of all of them was studied, leading to the conclusion that the most stable one is as shown in Fig. 1. The unit cell of $Mo_2Ga_2C$-ABA seen in Fig. 1 is in fact composed of two primitive cells on top of each other, but we chose to study it this way to enable a more direct comparison with $Mo_2Ga_2C$-ABC, upon consideration of the same number of atoms of each species and more similar box volumes.

The calculated band diagrams of $Mo_2Ga_2C$-ABC and $Mo_2Ga_2C$-ABA are shown in Fig. 2. The band structures of both carbides indicate that they display metallic nature. In the case of $Mo_2Ga_2C$-ABC, this is in consonance with the results of ref. 36, where a visually identical band structure of $Mo_2Ga_2C$ (ABC) was predicted.

Table 1 contains the calculated lattice parameters of the $Mo_2Ga_2C$ MAX phase with either atomic layer stacking, and of the same materials when all Ga atoms are replaced by O ones, generating a $Mo_2O_2C$ "MOX phase". The lattice parameters of $Mo_2Ga_2C$-ABC ($a$ = 3.07 Å and $c$ = 18.12 Å) are within 1% of the ones measured in ref. 21 ($a$ = 3.05 Å and $c$ = 18.19 Å), where the first synthesis of this MAX phase was reported. Notice that the lattice parameters $a$ and $c$ of $Mo_2Ga_2C$-ABA deviate from the experimental ones by −4% and +6%, respectively. In contrast, the calculated $a$ of $Mo_2O_2C$-ABA (2.89 Å), which resembles an ABA-stacked $Mo_2CO_2$ MXene, is in close agreement with the same parameter measured experimentally for the $Mo_2CT_x$ MXene in ref. 27 (2.86 Å), while the same parameter calculated for the MXene-like $Mo_2O_2C$-ABC (2.96 Å) differs from the experimental one by 4%. These results support the fact that synthesised $Mo_2Ga_2C$ MAX phases display an ABC atomic layer stacking in its $Mo_2C$ layers, assumed in the literature,[24,25] while the $Mo_2C$ MXenes produced by removing the Ga layers of $Mo_2Ga_2C$ have their atomic layers stacked in an ABA (hexagonal close-packed) arrangement.[12] The ABC stacking of experimentally obtained $Mo_2Ga_2C$ MAX phases is further supported by our calculated relative thermodynamic stability of the $Mo_2Ga_2C$-ABC and ABA models, which is 1.05 eV per unit cell in favour of the ABC-stacked model. This value changes by less than 0.1 eV with the inclusion of D3 dispersion corrections in the calculations.

If one includes D3 dispersion corrections to calculate the values in Table 1, the $a$ parameters are left unchanged, and the $c$ ones are reduced by 1 Å for $Mo_2O_2C$ only. As expected, the dispersion corrections have a greater effect on results relative to $Mo_2O_2C$. Nevertheless, the calculated $c$ lattice constants of $Mo_2O_2C$ are not relevant because, experimentally, the Ga-etching out of $Mo_2Ga_2C$ MAX phases originates MXenes in a solution with concomitant intercalation of solvent molecules and of other species present in the reaction medium (see, for example, Fig. 2 in ref. 37), so the measured $c$ parameters of $Mo_2CT_x$ are naturally much larger (20.5 Å and 24.7 Å in ref. 27 and 22, for example) than the ones predicted by calculations in vacuum.

From the data shown in Table 1, one additionally infers that the replacement of Ga atoms with O ones reduces the values of all the lattice parameters of the $Mo_2Ga_2C$ MAX phase, which was expected, given the reduced size of O atoms when

Table 1 Calculated lattice parameters of $Mo_2Ga_2C$. The notation $Mo_2O_2C$ represents $Mo_2Ga_2C$ models in which all Ga atoms were replaced by O ones, and the positions and cell size reoptimized. The values shown are for calculations without D3 dispersion corrections

| Material | $a = b$ (Å) | $c$ (Å) |
|---|---|---|
| $Mo_2Ga_2C$-ABC | 3.07 | 18.12 |
| $Mo_2Ga_2C$-ABA | 2.93 | 19.36 |
| $Mo_2O_2C$-ABC | 2.96 | 16.61 |
| $Mo_2O_2C$-ABA | 2.89 | 17.18 |

compared with that of Ga atoms. However, even when adding dispersion corrections in the calculations, which reduce the *c* lattice constants of $Mo_2O_2C$, the distance between nearest O atoms is greater than that the bond length of the Ga pairs. On $Mo_2Ga_2C$-ABC, the Ga–Ga distance was estimated at 2.49 Å, which increases to an O–O distance of 2.73 Å on $Mo_2O_2C$-ABC (with D3). Likewise, on $Mo_2Ga_2C$-ABA, the Ga–Ga distance was estimated at 2.51 Å, and increases to an O–O distance of 2.79 Å on $Mo_2O_2C$-ABA (with D3). This prompted us to calculate the binding energy of the $Mo_2O_2C$, *i.e.*, the energy per formula unit required to separate the $Mo_2O_2C$ MOX phase into individual $Mo_2CO_2$ MXene sheets, which can be calculated as half the energetic difference between a $Mo_2O_2C$ unit cell and two $Mo_2CO_2$ unit cells. The calculated binding energies are $-0.23$ and $-0.22$ eV for the ABC- and ABA-stacked models, suggesting that $Mo_2O_2C$ is in fact a van der Waals solid, formed by weakly interacting two-dimensional $Mo_2CO_2$ MXene layers. For comparison, the calculated binding energy per unit cell of the (three-dimensional) $Mo_2Ga_2C$ with respect to two (two-dimensional) $Mo_2CGa_2$ MXene-like sheets is $-1.14$ and $-1.55$ eV for the for the ABA- and ABC-stacked surfaces, respectively. Hence, the binding of $Mo_2Ga_2C$ is stronger than that of $Mo_2CO_2$, despite the larger *c* lattice parameter of the former. This also indicates that the decrease in this lattice parameter when transitioning from the MAX phase to the MXene is not due to stronger interaction between adjacent sheets, but instead can simply be due to the smaller size of O atoms when compared to Ga ones.

The coordinates of optimized 2 × 2 × 1 supercells of $Mo_2Ga_2C$ and $Mo_2O_2C$, with ABC and ABA atomic layer stacking, are included in the SI.

### O- and F-related point defects in the $Mo_2Ga_2C$ MAX phase

Since the synthesis method of the $Mo_2CT_x$ MXene involves the use of hydrofluoric acid and the resulting MXene is functionalized mostly by O groups with some F groups,[22,27] we investigated the interaction of O and F atoms with $Mo_2Ga_2C$ (with ABC atomic layer stacking, since we have established that this is the most accurate model). Three kinds of defects were analysed for each atom: interstitials ($O_{int}$ or $F_{int}$), Ga substitution ($O_{Ga}$ or $F_{Ga}$), and C substitution ($O_C$ or $F_C$). We considered Ga substitution because it is expected to occur naturally during the Ga-etching process, and C substitution because certain MAX phases are known to incorporate oxygen into their carbon sublattices, a characteristic that can be passed onto their corresponding A-element-etched MXene derivatives.[38–41] The interstitial O or F positions that were analysed involve bonding with at least one Ga atom of $Mo_2Ga_2C$, as was done, for example, in ref. 42 and 43 for self-interstitials and O and H interstitials in the $Ti_2AlN$ MAX phase. Therefore, five inequivalent interstitial sites were considered for O or F, as shown in Fig. 3. Three of these coincide with the interstitial sites in MAX phases with one atom of the A element per formula unit: the tetrahedral $Ga_3Mo$ (*i.e.*, O or F is inside a tetrahedron formed by three Ga atoms and one Mo atom) and $GaMo_3$ sites, and the octahedral $Ga_3Mo_3$ site. The other two interstitial sites are considered in this work for the first time because they are exclusive to MAX phases with more than one atom of the A element per formula unit, since they are located inside the triangular prisms formed by six Ga atoms.

The formation energies of each of these defects are given in Table 2. Note that using different species as reference can yield different formation energies. For example, in this work, the energy of a single F atom is $E(F) = E(HF) - E(H_2)/2$, but we could have simply done $E(F) = E(F_2)/2$, and this would lead to lower formation energies.[44] However, the predicted relative thermodynamic stability of the F-related defects would be the same. Thus, we conclude that, for both O- and F-related defects, the ones with the lowest formation energies are Ga substitutions, followed by O or F interstitials. In Table 2, only four rows of interstitial defects are shown because $O_{int}$ and $F_{int}$ at the $Ga_6$(Mo) site are not stable and, upon relaxation, become $Ga_3Mo$. Interstitial oxygen atoms are indeed present in some MAX phases, such as $Ti_2AlN$.[43] The formation energy of $F_C$ is considerably higher than any other value in Table 2, which might be a reason why, although HF is used to produce MXenes, oxycarbide and oxynitride MXenes have been observed, while no fluorocarbide or fluoronitride ones have been reported.

Structurally, $O_{Ga}$ and $F_{Ga}$ are significantly different. As shown in Fig. 4, a substitutional O binds to three Mo atoms of the nearest $Mo_2C$ slab, and its position relative to the nearest $Mo_2C$ slab is analogous to the FCC-like site where surface

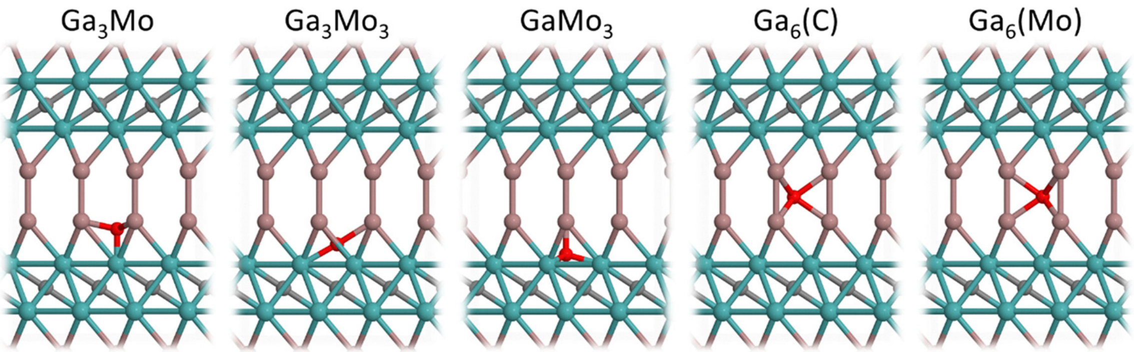

Fig. 3 Possible interstitial sites for O or F (only O shown here). Colour code for the spheres: Mo in cyan, Ga in pink, C in grey, O in red.

Table 2 Formation energies ($E_{form}$) of O- and F-related single-site point defects in the $Mo_2Ga_2C$ MAX phase. The lowest formation energy among the defects related to each atom is written in bold font

| O defects | | F defects | |
|---|---|---|---|
| Site | $E_{form}$ (eV) | Site | $E_{form}$ (eV) |
| $O_{int}$ $Ga_3Mo$ | −2.01 | $F_{int}$ $Ga_3Mo$ | +0.54 |
| $O_{int}$ $Ga_3Mo_3$ | −1.00 | $F_{int}$ $Ga_3Mo_3$ | +1.99 |
| $O_{int}$ $GaMo_3$ | −0.37 | $F_{int}$ $GaMo_3$ | +3.37 |
| $O_{int}$ $Ga_6(C)$ | −0.14 | $F_{int}$ $Ga_6(C)$ | +1.60 |
| $O_{Ga}$ | **−2.65** | $F_{Ga}$ | **−0.68** |
| $O_C$ | −0.74 | $F_C$ | +4.14 |

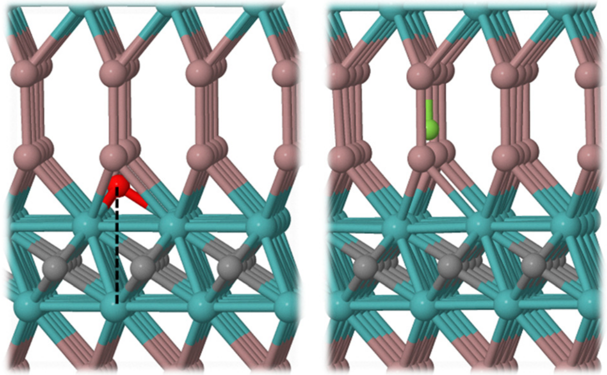

Fig. 4 Structures of the Ga-substitutional O (left) and Ga-substitutional F (right) defects in $Mo_2Ga_2C$. The dashed line shows the vertical alignment between the O atom and the farthest Mo atom of the nearest $Mo_2C$ slab. Colour code for the spheres: Mo in cyan, Ga in pink, C in grey, O in red, F in green.

terminations are preferably located on most MXenes, *i.e.*, a hollow surface site above an atom of the M element.[8,45] The $O_{Ga}$ atom is substantially closer (downwards in Fig. 4, by 1.1 Å) to the $Mo_2C$ slab than the Ga atom was. In turn, a substitutional $F_{Ga}$ atom in the $Mo_2Ga_2C$ lattice prefers to move 0.8 Å away (upwards in Fig. 4) from the nearest $Mo_2C$ planes and bind to the other Ga atom of the Ga–Ga pair. Possibly, this is related to HF being so successful in breaking Ga–Mo bonds and etching out the Ga layers, to the more prominent occurrence of an O surface termination (80%), when compared to F (10%), in the synthesised $Mo_2C$ MXene reported in ref. 22. Furthermore, the fact that substitutional F atoms bind to Ga atoms in $Mo_2Ga_2C$, at least during the initial stages of Ga etching, suggests that Ga atoms may be removed in the form of an incipient gallium fluoride species, such as trigonal $GaF_3$, the most stable gallium fluoride, in analogy with the aluminium fluoride ($AlF_3$) that forms when synthesising $Ti_3C_2$ from the $Ti_3AlC_2$ MAX phase.

According to our calculations, many of the defects studied here attract each other, as illustrated in Fig. 5. This is true for substitutional O atoms, for which the energetic difference between two O atoms replacing two Ga atoms of the same Ga–Ga pair, and replacing two Ga atoms far from each other, is 1.21 eV in favour of the former. This makes sense from the point of view of chemical bonds: replacing a Ga–Ga pair by an O–O pair requires breaking six Ga–Mo bonds and one Ga–Ga one, while replacing two Ga atoms by two O atoms far from each other requires breaking six Ga–Mo bonds and two Ga–Ga ones, *i.e.*, one more Ga–Ga bond. We verified this by comparing the energy of two Ga vacancies far from each other, with that of a Ga–Ga pair vacancy, and found the latter is more stable by 1.20 eV, implying that Ga vacancies attract each other as well. Equivalently, this energy can be used as an estimate of the Ga–Ga bond energy in $Mo_2Ga_2C$. The 1.20 eV value is within the calculated binding energies per unit cell of ABA- and ABC-stacked surfaces of $Mo_2Ga_2C$ reported above. Curiously, we found that pairs of substitutional O atoms are also thermodynamically more stable when next to each other. All these results suggest a cascading effect when etching out the Ga layers of $Mo_2Ga_2C$, wherein regions of the material adjacent to where Ga atoms have been replaced by O ones are more prone to have their Ga content replaced by O as well. Hence, as Ga atoms are etched out of the $Mo_2Ga_2C$ MAX phase, O atoms from O-containing species in solution occupy neighbouring Ga sites, serving as the surface termination of the $Mo_2C$ MXene that is eventually formed.

Although the $Mo_2C$ MXene has been synthesised numerous times since the discovery of the $Mo_2Ga_2C$ MAX phase,[22] attempts to obtain it from the $Mo_2GaC$ MAX phase have proved elusive. For comparison, we analysed the structure of a Ga-substituting O atom in $Mo_2GaC$, using the same simulation parameters as for $Mo_2Ga_2C$, but with a model containing only one Ga atomic layer between each pair of $Mo_2C$ slabs. As shown in Fig. S1, we observed that the most stable position of $O_{Ga}$ in $Mo_2GaC$ is amid the Ga layer, bonded to two Ga atoms, contrasting with the same defect in $Mo_2Ga_2C$, in which $O_{Ga}$ binds to the three nearest Mo atoms. It is well known that MXenes are enormously stabilized when their surfaces are functionalized. Therefore, it is possible that, in order to produce the $Mo_2C$ MXene (and possibly other MXenes) from a MAX phase, having O atoms serving as the surface termination of the MXene is a requirement to stabilize the new 2D material and produce the cascading effect mentioned in the previous paragraph.

### Atomic layer stacking stability in the $Mo_2Ga_2C$ MAX phase with increasing O content

After having found a mechanism *via* which the Ga atoms of $Mo_2Ga_2C$ can sequentially be replaced by O ones, we investigated the relative stability of the ABC- and ABA-stacked $Mo_2Ga_2C$ MAX phase models with varying $O_{Ga}$ content. To this end, we used the total energies of optimized models that contain 2 × 2 × 1 unit cells of $Mo_2Ga_2C$, in which different numbers of pairs of Ga atoms have been replaced by pairs of O atoms. Each unit cell contains two Ga–Ga pairs, allowing us to assess seven O concentrations between 0% ($Mo_2Ga_2C$) and 100% ($Mo_2O_2C$). As mentioned in the section with the computational methods, three approaches were considered separately: one without D3 dispersion corrections and a fixed supercell size, another with D3 corrections and fixed supercell size, and a final one including D3 corrections and optimizing the supercell size for each O concentration. The third of these methods is expected to yield the most reliable results, because we have

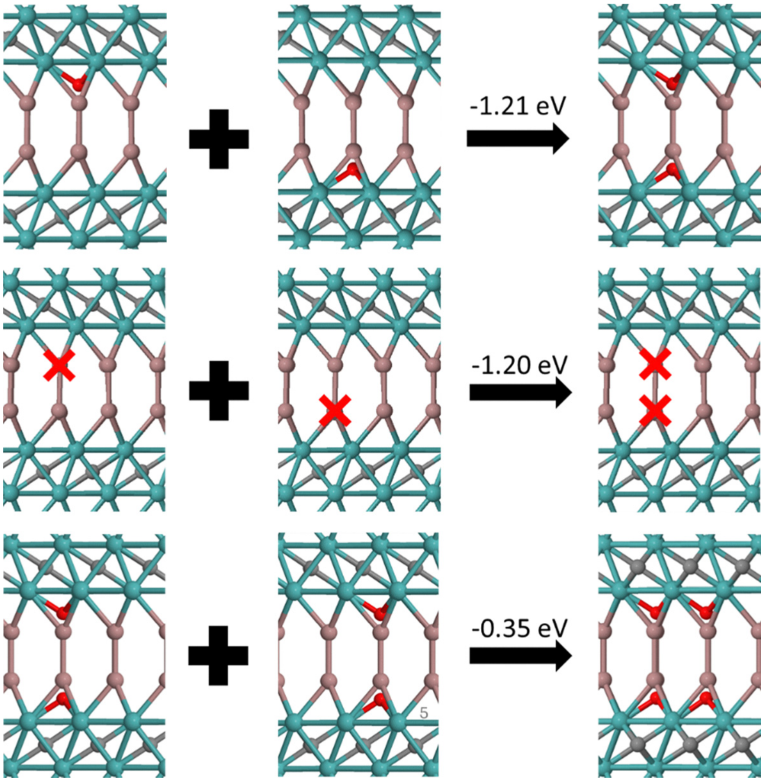

**Fig. 5** Illustration of the attraction between single substitutional O atoms (top panels), single Ga vacancies (middle panels), and pairs of substitutional O atoms (bottom panels) in $Mo_2Ga_2C$. Colour code for the spheres: Mo in cyan, Ga in pink, C in grey, O in red. The red crosses denote Ga vacancies.

determined that $Mo_2O_2C$ is a van der Waals solid and because the lattice parameters should need to adapt to the replacement of Ga atoms by O ones.

The comparison of the relative stability of the ABC and ABA phases of the $Mo_2Ga_{2-x}O_xC$ models can be made with the aid of Fig. 6. In this Figure, we find that the data obtained using all three methods described in the previous paragraph are nearly coincident, which suggests that van der Waals interactions have only a small effect on the lattice constants. In the $Mo_2Ga_2C$ MAX phase, the ABC atomic layer stacking is more

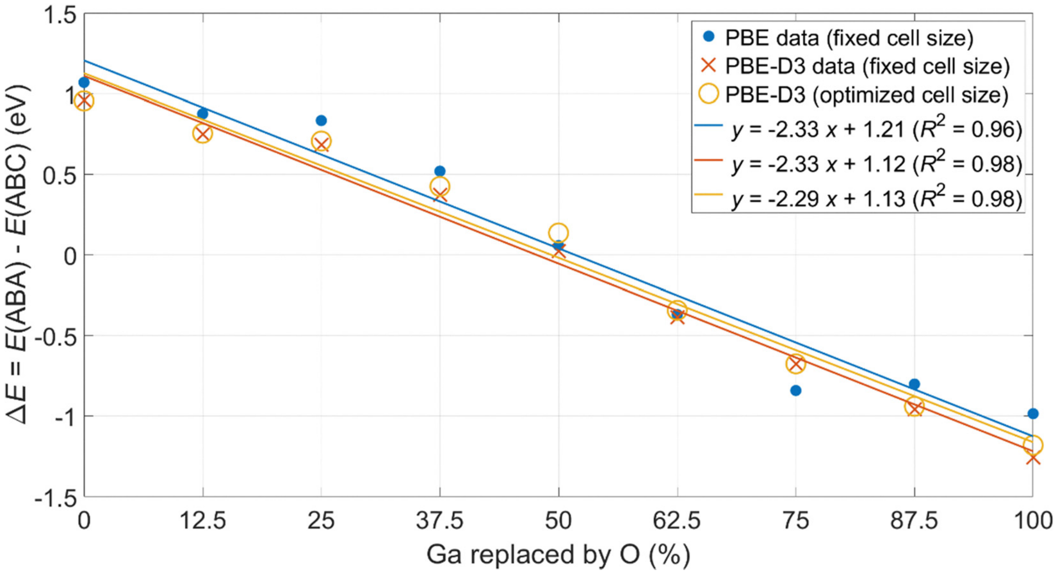

**Fig. 6** Energetic difference per unit cell ($\Delta E$) between the $Mo_2Ga_2C$ MAX phase with ABA and ABC atomic layer stacking, as a function of the percentage of Ga atoms that are replaced by O ones: 0 corresponds to the pristine $Mo_2Ga_2C$ MAX phase, 100 to the $Mo_2O_2C$ MOX phase, and values between 0 and 100 to intermediate O/Ga content.

stable than the ABA one by just over 1 eV, whereas if all the Ga content is replaced by O, this difference is reversed, with the ABA alignment being preferred by just over 1 eV. The results generate approximately symmetric linear relations around 50% replacement of Ga by O, the point near which the phase transition occurs.

## Summary and conclusions

In this work, we employed density-functional theory (DFT) calculations using the PBE exchange–correlation functional, both with and without D3 dispersion corrections, as implemented in the VASP code, to investigate the transformation of the $Mo_2Ga_2C$ MAX phase into the $Mo_2C$ MXene. Our results provide thermodynamic and structural insights into the etching process of Ga and subsequent surface functionalization by O atoms, with a focus on the evolution of atomic stacking sequences and defect energetics.

We found that the pristine $Mo_2Ga_2C$ MAX phase exhibits an ABC stacking of its atomic layers, in agreement with experimental data and previous theoretical work. As Ga atoms are progressively replaced by oxygen, the ABA stacking becomes increasingly favourable, with a crossover in stability occurring near 50% Ga-to-O substitution. This concentration marks a critical point for the phase transition from the ABC to the ABA configuration, which is energetically preferred for the resulting $Mo_2CO_2$ MXene by more than 1 eV per unit cell. The O substitution leads to a contraction of the lattice, as expected due to the smaller atomic size of oxygen compared to gallium. The calculated binding energies between the interacting $Mo_2CO_2$ MXene sheets are of about 0.2 eV per formula unit, which suggests a classification as a van der Waals solid of the material derived from the pristine $Mo_2Ga_2C$ MAX phase upon full Ga-to-O substitution. The results suggest that transformation from the ABA MAX phase to the MXene phase is thermodynamically favorable but, the replacement of Ga by O is expected to involve an energy barrier, as it requires chemical transformation and likely the breaking and formation of bonds.

By evaluating the formation energies of O and F atoms placed at three types of defect sites, namely, interstitial, Ga-substituted, and C-substituted, we found the stability to follow the order: Ga-substituted > interstitial > C-substituted, for both elements. Fluorine was consistently less thermodynamically favourable than oxygen. Notably, when replacing Ga, it was found that oxygen atoms occupy sites analogous to the FCC hollow positions typically favoured by surface terminations in MXenes, whereas fluorine atoms preferentially bond with remaining Ga atoms. This suggests the formation of incipient gallium fluoride species during the etching process, aligning with experimental findings for the $Ti_3AlC_2$ MAX phase, where Al is removed in the form of $AlF_3$. Furthermore, the energetic analysis reveals that oxygen substitutions are more stable when occupying adjacent Ga–Ga pairs, indicating a cooperative or cascading mechanism during etching. These results support a defect-driven structural transition, in which O atoms preferentially and locally replace Ga, thereby stabilizing neighbouring sites for subsequent substitution and promoting the progression of the Ga etching process.

Overall, our calculations shed light on the atomistic mechanisms driving the transformation of $Mo_2Ga_2C$ into the $Mo_2C$ MXene under HF-based etching conditions, offering a theoretical explanation for the experimentally observed predominance of oxygen terminations and the associated structural shift from ABC to ABA stacking. The close agreement between our results and experimental findings strengthens the mechanistic understanding of this MXene synthesis pathway. Building on this foundation, further computational studies may help design alternative etching strategies that promote targeted surface terminations or stacking arrangements, potentially enabling the synthesis of MXenes that have so far remained experimentally elusive.

## Conflicts of interest

There are no conflicts of interest to declare. The authors declare no competing interests.

## Data availability

The data supporting this article have been included as part of the SI, which includes a representation of the structure of $O_{Ga}$ in $Mo_2GaC$, and coordinates of optimized 2 × 2 × 1 supercells of $Mo_2Ga_2C$ and $Mo_2O_2C$, either with ABC or ABA atomic layer stacking. See DOI: **https://doi.org/10.1039/d5cp02315g**

## Acknowledgements

This work was developed within the scope of the projects CICECO-Aveiro Institute of Materials, with ref. UIDB/50011/2020, UIDP/50011/2020 and LA/P/0006/2020, HydroFormX with ref. 2023.12765.PEX, and CRF – CRG 2022 KAUST with ref. ORFS-2022-CRG11-5075.2. We are also thankful to FCT I. P. for the computational resources granted in the framework of project ref. 2024.13633.CPCA.A3 by the FCT 2024 Call for Advanced Computing Projects. JDG thanks the Portuguese Foundation for Science and Technology (FCT) through the grant with ref. 2023.06511.CEECIND, in the scope of the Individual Call to Scientific Employment Stimulus – 6th Edition.

## References

1 M. Dahlqvist, M. W. Barsoum and J. Rosen, MAX phases – Past, present, and future, *Mater. Today*, 2024, **72**, 1–24, DOI: **10.1016/j.mattod.2023.11.010**.

2 M. Naguib, M. Kurtoglu, V. Presser, J. Lu, J. Niu, M. Heon, L. Hultman, Y. Gogotsi and M. W. Barsoum, Two-Dimensional Nanocrystals Produced by Exfoliation of $Ti_3AlC_2$, *Adv. Mater.*, 2011, **23**, 4248–4253, DOI: **10.1002/adma.201102306**.

3 M. Rahman and M. S. Al Mamun, Future prospects of MXenes: synthesis, functionalization, properties, and application in field effect transistors, *Nanoscale Adv.*, 2024, **6**, 367–385, DOI: **10.1039/D3NA00874F**.

4 H. Rohde and V. H. Kudielka, Strukturuntersuchungen an carbosulfiden von titan und zirkon, *Z. Krist.*, 1960, **114**, 447, DOI: **10.1524/zkri.1960.114.16.447**.

5 J. D. Gouveia, G. Novell-Leruth, P. M. L. S. Reis, F. Viñes, F. Illas and J. R. B. Gomes, First-Principles Calculations on the Adsorption Behavior of Amino Acids on a Titanium Carbide MXene, *ACS Appl. Bio Mater.*, 2020, **3**, 5913–5921, DOI: **10.1021/acsabm.0c00621**.

6 J. D. Gouveia, G. Novell-Leruth, F. Viñes, F. Illas and J. R. B. Gomes, The $Ti_2CO_2$ MXene as a nucleobase 2D sensor: a first-principles study, *Appl. Surf. Sci.*, 2021, **544**, 148946, DOI: **10.1016/j.apsusc.2021.148946**.

7 J. D. Gouveia and J. R. B. Gomes, Adsorption of Hexoses on the $Ti_2CO_2$ MXene, *J. Phys. Chem. C*, 2024, **128**, 20369–20377, DOI: **10.1021/acs.jpcc.4c04821**.

8 J. D. Gouveia and J. R. B. Gomes, Effect of the surface termination on the adsorption of flue gas by the titanium carbide MXene, *Mater. Today Chem.*, 2023, **29**, 101441, DOI: **10.1016/j.mtchem.2023.101441**.

9 J. D. Gouveia, H. Rocha and J. R. B. Gomes, MXene-supported transition metal single-atom catalysts for nitrogen dissociation, *Mol. Catal.*, 2023, **547**, 113373, DOI: **10.1016/j.mcat.2023.113373**.

10 J. D. Gouveia, Á. Morales-García, F. Viñes, J. R. B. Gomes and F. Illas, Facile Heterogeneously Catalyzed Nitrogen Fixation by MXenes, *ACS Catal.*, 2020, **10**, 5049–5056, DOI: **10.1021/acscatal.0c00935**.

11 J. D. Gouveia, Á. Morales-García, F. Viñes, F. Illas and J. R. B. Gomes, MXenes as promising catalysts for water dissociation, *Appl. Catal., B*, 2020, **260**, 118191, DOI: **10.1016/j.apcatb.2019.118191**.

12 J. D. Gouveia and J. R. B. Gomes, The determining role of $T_x$ species in the catalytic potential of MXenes: water adsorption and dissociation on $Mo_2CT_x$, *Catal. Today*, 2023, **424**, 113848, DOI: **10.1016/j.cattod.2022.07.016**.

13 S. Saharan, U. Ghanekar and S. Meena, $V_2N$ MXene for Hydrogen Storage: First-Principles Calculations, *J. Phys. Chem. C*, 2024, **128**, 1612–1620, DOI: **10.1021/acs.jpcc.3c07786**.

14 T. Thomas, S. Bontha, A. Bishnoi and P. Sharma, MXene as a hydrogen storage material? A review from fundamentals to practical applications, *J. Energy Storage*, 2024, **88**, 111493, DOI: **10.1016/j.est.2024.111493**.

15 P. Kumar, S. Singh, S. A. R. Hashmi and K.-H. Kim, MXenes: emerging 2D materials for hydrogen storage, *Nano Energy*, 2021, **85**, 105989, DOI: **10.1016/j.nanoen.2021.105989**.

16 N. Li, J. Peng, W.-J. Ong, T. Ma, Arramel, P. Zhang, J. Jiang, X. Yuan and C. (John) Zhang, MXenes: An Emerging Platform for Wearable Electronics and Looking Beyond, *Matter*, 2021, **4**, 377–407, DOI: **10.1016/j.matt.2020.10.024**.

17 D. Ayodhya, A review of recent progress in 2D MXenes: synthesis, properties, and applications, *Diamond Relat. Mater.*, 2023, **132**, 109634, DOI: **10.1016/j.diamond.2022.109634**.

18 D. Dhamodharan, M. A. Al-Harthi, B. Ramya, A. Bafaqeer and F. Alam, MXenes: a promising material with multifunctional applications, *J. Environ. Chem. Eng.*, 2024, **12**, 112316, DOI: **10.1016/j.jece.2024.112316**.

19 H. Kim and H. N. Alshareef, MXetronics: MXene-Enabled Electronic and Photonic Devices, *ACS Mater. Lett.*, 2020, **2**, 55–70, DOI: **10.1021/acsmaterialslett.9b00419**.

20 L. E. Toth, High superconducting transition temperatures in the molybdenum carbide family of compounds, *J. Less Common Met.*, 1967, **13**, 129–131, DOI: **10.1016/0022-5088(67)90055-0**.

21 C. Hu, C.-C. Lai, Q. Tao, J. Lu, J. Halim, L. Sun, J. Zhang, J. Yang, B. Anasori, J. Wang, Y. Sakka, L. Hultman, P. Eklund, J. Rosen and M. W. Barsoum, $Mo_2Ga_2C$: a new ternary nanolaminated carbide, *Chem. Commun.*, 2015, **51**, 6560–6563, DOI: **10.1039/C5CC00980D**.

22 R. Meshkian, L.-Å. Näslund, J. Halim, J. Lu, M. W. Barsoum and J. Rosen, Synthesis of two-dimensional molybdenum carbide, $Mo_2C$, from the gallium based atomic laminate $Mo_2Ga_2C$, *Scr. Mater.*, 2015, **108**, 147–150, DOI: **10.1016/j.scriptamat.2015.07.003**.

23 Y. Guo, S. Jin, L. Wang, P. He, Q. Hu, L.-Z. Fan and A. Zhou, Synthesis of two-dimensional carbide $Mo_2CT_x$ MXene by hydrothermal etching with fluorides and its thermal stability, *Ceram. Int.*, 2020, **46**, 19550–19556, DOI: **10.1016/j.ceramint.2020.05.008**.

24 M. A. Hadi, New ternary nanolaminated carbide $Mo_2Ga_2C$: a first-principles comparison with the MAX phase counterpart $Mo_2GaC$, *Comput. Mater. Sci.*, 2016, **117**, 422–427, DOI: **10.1016/j.commatsci.2016.02.018**.

25 C.-C. Lai, R. Meshkian, M. Dahlqvist, J. Lu, L.-Å. Näslund, O. Rivin, E. N. Caspi, O. Ozeri, L. Hultman, P. Eklund, M. W. Barsoum and J. Rosen, Structural and chemical determination of the new nanolaminated carbide $Mo_2Ga_2C$ from first principles and materials analysis, *Acta Mater.*, 2015, **99**, 157–164, DOI: **10.1016/j.actamat.2015.07.063**.

26 J. D. Gouveia, F. Viñes, F. Illas and J. R. B. Gomes, MXenes atomic layer stacking phase transitions and their chemical activity consequences, *Phys. Rev. Mater.*, 2020, **4**, 054003, DOI: **10.1103/PhysRevMaterials.4.054003**.

27 E. B. Deeva, A. Kurlov, P. M. Abdala, D. Lebedev, S. M. Kim, C. P. Gordon, A. Tsoukalou, A. Fedorov and C. R. Müller, In Situ XANES/XRD Study of the Structural Stability of Two-Dimensional Molybdenum Carbide $Mo_2CT_x$: Implications for the Catalytic Activity in the Water–Gas Shift Reaction, *Chem. Mater.*, 2019, **31**, 4505–4513, DOI: **10.1021/acs.chemmater.9b01105**.

28 G. Kresse and J. Furthmüller, Efficient iterative schemes for ab initio total-energy calculations using a plane-wave basis set, *Phys. Rev. B: Condens. Matter Mater. Phys.*, 1996, **54**, 11169–11186, DOI: **10.1103/PhysRevB.54.11169**.

29 J. P. Perdew, K. Burke and M. Ernzerhof, Generalized Gradient Approximation Made Simple, *Phys. Rev. Lett.*, 1996, **77**, 3865–3868, DOI: **10.1103/PhysRevLett.77.3865**.

30 P. E. Blöchl, Projector augmented-wave method, *Phys. Rev. B: Condens. Matter Mater. Phys.*, 1994, **50**, 17953–17979, DOI: **10.1103/PhysRevB.50.17953**.

31 S. Grimme, J. Antony, S. Ehrlich and H. Krieg, A consistent and accurate ab initio parametrization of density functional dispersion correction (DFT-D) for the 94 elements H-Pu, *J. Chem. Phys.*, 2010, **132**, 154104, DOI: **10.1063/1.3382344**.

32 J. D. Gouveia, T. L. P. Galvão, K. Iben Nassar and J. R. B. Gomes, First-principles and machine-learning approaches for interpreting and predicting the properties of MXenes, *npj 2D Mater. Appl.*, 2025, **9**, 8, DOI: **10.1038/s41699-025-00529-5**.

33 A. S. Tygesen, M. Pandey, T. Vegge, K. S. Thygesen and J. M. García-Lastra, Role of Long-Range Dispersion Forces in Modeling of MXenes as Battery Electrode Materials, *J. Phys. Chem. C*, 2019, **123**, 4064–4071, DOI: **10.1021/acs.jpcc.8b11663**.

34 J. Liu, T. Shen, J.-C. Ren, S. Li and W. Liu, Role of van der Waals interactions on the binding energies of 2D transition-metal dichalcogenides, *Appl. Surf. Sci.*, 2023, **608**, 155163, DOI: **10.1016/j.apsusc.2022.155163**.

35 H. J. Monkhorst and J. D. Pack, Special points for Brillouin-zone integrations, *Phys. Rev. B: Condens. Matter Mater. Phys.*, 1976, **13**, 5188–5192, DOI: **10.1103/PhysRevB.13.5188**.

36 M. Nadeem, M. Haseeb, A. Hussain, A. Javed, M. A. Rafiq, M. Ramzan, M. N. Rasul and M. A. Khan, Structural stability, electronic structure, mechanical and optical properties of MAX phase ternary $Mo_2Ga_2C$, $Mo_2GaC$ and $Mo_3GaC_2$ carbides, *J. Mater. Res. Technol.*, 2021, **14**, 521–532, DOI: **10.1016/j.jmrt.2021.06.079**.

37 B. Anasori, M. R. Lukatskaya and Y. Gogotsi, 2D metal carbides and nitrides (MXenes) for energy storage, *Nat. Rev. Mater.*, 2017, **2**, 16098, DOI: **10.1038/natrevmats.2016.98**.

38 P. P. Michałowski, M. Anayee, T. S. Mathis, S. Kozdra, A. Wójcik, K. Hantanasirisakul, I. Jóźwik, A. Piątkowska, M. Możdżonek, A. Malinowska, R. Diduszko, E. Wierzbicka and Y. Gogotsi, Oxycarbide MXenes and MAX phases identification using monoatomic layer-by-layer analysis with ultralow-energy secondary-ion mass spectrometry, *Nat. Nanotechnol.*, 2022, **17**, 1192–1197, DOI: **10.1038/s41565-022-01214-0**.

39 P. P. Michałowski, Unraveling the composition of each atomic layer in the MXene/MAX phase structure – identification of oxycarbide, oxynitride, and oxycarbonitride subfamilies of MXenes, *Nanoscale Horiz.*, 2024, **9**, 1493–1497, DOI: **10.1039/D4NH00151F**.

40 J. D. Gouveia and J. R. B. Gomes, Structural and electronic properties of the titanium carbide MXene with variable sublattice oxygen composition, *Surf. Interfaces*, 2024, **46**, 103920, DOI: **10.1016/j.surfin.2024.103920**.

41 J. D. Gouveia and J. R. B. Gomes, Effect of surface composition on the stability of Ti- and V-based oxycarbide and oxynitride MXenes, *Mater. Today Phys.*, 2024, **46**, 101481, DOI: **10.1016/j.mtphys.2024.101481**.

42 J. Z. Duan, J. R. Zhang, C. L. Wang, Y. Qiu, W. S. Duan and L. Yang, First principles investigation of point defect-related properties in $Ti_2AlN$, *RSC Adv.*, 2014, **4**, 42014–42021, DOI: **10.1039/C4RA07200F**.

43 F. Colonna and C. Elsässer, First principles DFT study of interstitial hydrogen and oxygen atoms in the MAX phase $Ti_2AlN$, *RSC Adv.*, 2017, **7**, 37852–37857, DOI: **10.1039/C7RA05045C**.

44 J. D. Gouveia and J. R. B. Gomes, Structural and energetic properties of vacancy defects in MXene surfaces, *Phys. Rev. Mater.*, 2022, **6**, 024004, DOI: **10.1103/PhysRevMaterials.6.024004**.

45 J. Björk and J. Rosen, Functionalizing MXenes by Tailoring Surface Terminations in Different Chemical Environments, *Chem. Mater.*, 2021, **33**, 9108–9118, DOI: **10.1021/acs.chemmater.1c01264**.